Model of an Ironless Axial Flux Permanent Magnet Motor Based on the Field Produced by a Single Magnet

Maxime Bonnet, Yvan Lefèvre, Jean-François Llibre, Dominique Harribey, François Defay

Model of an Ironless Axial Flux Permanent Magnet Motor Based on the Field Produced by a Single Magnet

Maxime Bonnet[1], Yvan Lefèvre[1], Jean-François Llibre[1], Dominique Harribey[1] and François Defay[2]

[1]LAPLACE, Université de Toulouse, CNRS, INPT, UPS, France
[2]ISAE-SUPAERO, Université de Toulouse, Toulouse, France

The Lorentz force law is proposed as an alternative to the Maxwell stress tensor to calculate the torque of an ironless Axial Flux Permanent Magnet motor. This alternative allows calculating only the magnetic field produced by the magnets. A model of this magnetic field based on the field produced by one magnet, the superposition principle and geometric transformations is proposed. A method for calculating the magnetic field of this single magnet, inspired by finite elements, is proposed to reduce the calculation time. The method is validated by 3D Finite Element Analysis simulations and experimental measurements performed on a test bench.

***Index Terms*— Axial Flux Permanent Magnet, Integral formulation, Ironless, Lorentz force law, Torque.**

I. Introduction

Ironless Axial Flux Permanent Magnet (AFPM) motors have high torque density. Applications such as aeronautics are seeking to use ironless-stator AFPM motor [1]. However, ironless AFPM motors have two main drawbacks: their design and manufacture. Thanks to additive manufacturing, new markets for AFPM motors may be opened up [2].

Unfortunately, additively manufactured irons are still under study [3]. Additively manufacturing ironless AFPM motor is easier. However, its sizing is still complex because of the lack of analytical models. Without iron, the integral formulations based on Coulomb's law are a good alternative to 3D Finite Element Analysis (3D FEA) [4]. In this article, a model of the open circuit magnetic field based on the calculation of the field of a single magnet by integral formulation is proposed to size this type of motor. The total field due to all magnets is obtained by using the linear superposition principle [5-8].

The analytical formulation of the integrals gives accurate results. To speed up the calculation, these integrals are transformed in matrix products by the use of the nodal approximation method like in finite element method [9]. The geometrical symmetries are taken into account to more reduce the computation times. The use of matrix products combined with geometrical transformations to provide a fast characterization of ironless AFPM constitutes the main contribution of this paper.

In section II the studied motor is presented first before the description of the nodal method in section III. The section IV shows the use of the geometrical transformations with the linear superposition principle. Section V is dedicated to 3D FEA and experimental validations of the method with the studied motor.

II. Prototype Characteristics

The method is applied on a three-phase ironless AFPM motor with a double rotor and a single stator (Fig. 1) [10]. This motor is designed to test the additive manufacturing. The magnets are cylindrical for cost reasons with a polarisation J_r = 1.31 T and a relative permeability μ_{ra} = 1.14 [12]. The double rotor is chosen to increase the open circuit magnetic field applied on stator coils. The stator consists of two stages of six coils. The sizes of the active parts are described in Table I.

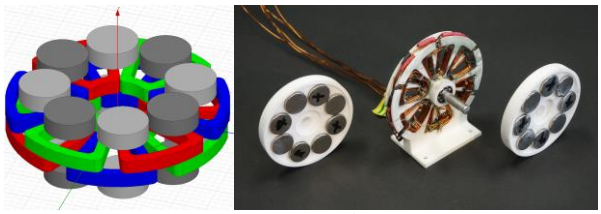

Fig. 1. Prototype on ANSYS-Maxwell [11] (left) and in picture (right)

The non-active parts of this prototype are additively manufactured with nylon polyamide PA 2200 [13]. The complete assembly of this prototype is illustrated on video [14].

TABLE I
DIMENSIONS OF THE ACTIVE PARTS OF THE PROTOTYPE

Magnet N_dF_eB N42 [12]	Diameter (mm)		15
	Height (mm)		5
	Pole Pairs	p	4
	Pole pitch (degree)	$\alpha = \pi/p$	*45*
	Number of rotor	n_r	*2*
	Number of magnets/rotor	$N_a=2p$	*8*
	Distance between rotors (mm)	z_1	*10*
	Air gap (mm)	g	*1*
Coil	Internal Radius (mm)		9.29
	External Radius (mm)		32.5
	Slot thickness (mm)		2.90
	Height (mm)		4
	Opening angle (degree)		45
	Total number of slots	n_e	24
	Conductors/slot	n_c	12
	Phases	q	3
	Slots/pole/phase	m	1

III. Integral Formulation using Nodal Approximation

A. Integral formulation

In this section, line vectors are denoted with <> and column vectors with {}. To calculate the open circuit magnetic field generated by magnets, the Coulombian model as presented in [4] is applied. This field is calculated on target points located on coils. The magnetization $\overrightarrow{M}$ is considered uniform in all magnets. The sources of the open circuit magnetic field are the surface charge densities σ on their external surfaces Σ:

$$\sigma = \vec{M}.\vec{n} = \vec{J}_r.\vec{n} \Big/ \mu_0 \mu_{r_a} \quad (1)$$

The expression of the magnetic excitation field $\vec{H}$ created on a target point *C* is given by (2) and (3) where *S* is a source point belonging to the external surfaces Σ of the magnet:

$$\vec{H^C} = \frac{\sigma}{4\pi} \iint_{S \in \Sigma} \vec{u_{ex}}\left(\vec{x_S}, \vec{x_C}\right) d\Sigma \quad (2)$$

$$\vec{u_{ex}}\left(\vec{x_s}, \vec{x_c}\right) = \frac{\vec{r_{SC}}}{r_{SC}^3} = \frac{\langle x_c - x_s \quad y_c - y_s \quad z_c - z_s \rangle}{\left[(x_c - x_s)^2 + (y_c - y_s)^2 + (z_c - z_s)^2\right]^{3/2}} \quad (3)$$

B. Nodal approximation

The external surfaces with non-null surface charge density are meshed with n_m 2D quadrilateral elements and n_o nodes as in finite element method [9]. A single reference element with $n = 8$ nodes is defined to make quadratic approximations for all meshes. Local coordinates (ξ,η) and interpolation function $N_k(\xi,\eta)$ are defined on this reference element on each node *k*. Isoparametric elements are used so geometrical transformations can be defined between the local coordinates in the reference element and the real coordinates in each element of the external surfaces Σ [9]:

$$\tau : (\xi,\eta) \rightarrow \vec{x}(\xi,\eta) = \langle N(\xi,\eta) \rangle \left\{ \vec{x_n} \right\} \quad (4)$$

On each element *j*, the function defined by (3) is evaluated exactly on its nodes. Interpolation function $N_k(\xi,\eta)$ are used to obtain an approximation of this function on each point inside element *j* [9]:

$$\vec{u_{ex}}\left(\vec{\xi}, \vec{x_C}\right)_j \approx \vec{\tilde{u}}\left(\vec{\xi}, \vec{x_C}\right)_j = \langle N(\xi,\eta) \rangle \left\{ \vec{u_n}\left(\vec{x_C}\right) \right\}_j \quad (5)$$

The transformation (4) is applied to (2) for each element *j*. The field produced by the element *j*, H_j^C is given by:

$$\vec{H_j^C} = \frac{\sigma}{4\pi} \int_{-1}^{1} \int_{-1}^{1} \vec{u_{ex}}\left(\vec{x_S}(\xi,\eta), \vec{x_C}\right)_j \det(J)_j \, d\xi d\eta \quad (6)$$

The approximate function can then be written by combining (5) and (6):

$$\vec{\tilde{H}_j^C} = \left\langle q_{1_j} \quad \cdots \quad q_{n_j} \right\rangle \left\{ \vec{u_n}\left(\vec{x_C}\right) \right\}_j \quad (7)$$

$$q_{k_j} = \frac{\sigma}{4\pi} \int_{-1}^{1} \int_{-1}^{1} N_k(\xi,\eta) \det(J)_j \, d\xi d\eta \quad (8)$$

The total magnetic field is the sum of the magnetic field on point *C* produced by each element. The assembly method [9] is used to place the different elemental integral q_{kj} and the components of the elemental *u* vector (7) respectively in a global 1x n_o line matrix <*Q*> and n_o x3 three columns vector *u* (9):

$$\vec{\tilde{H}^C} = \langle Q \rangle \left\{ \vec{u}\left(\vec{x_C}\right) \right\} \quad (9)$$

The originality and the efficiency brought by (9) is that only the source nodes are involved in <*Q*>. This means that for a given magnet at a given position, it is possible to know the *H*-field at any point without having to recalculate <*Q*>. <*Q*> is calculated only once. The calculation of the matrix product (9) is very fast in the framework of Matlab.

C. Validation of nodal method

The magnetic field of one single magnet of the prototype is calculated using this method and compared to a 3D FEA performed with ANSYS [11]. The study domain is constituted by the single magnet in an air box where the furthest node is considered to be at infinity. The scalar potential is imposed zero on the latter. The air box has ten times the sizes of the magnet located in its center. The field is calculated on target points on five different surfaces located at different distances above the top of the. The magnetic field, calculated by the nodal method, on a surface above the top surface of the cylindrical magnet is shown on Fig. 2.

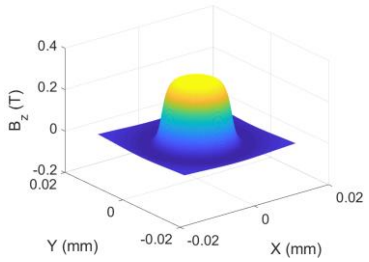

Fig. 2. Magnetic field produced by a cylindrical magnet on a surface above it.

TABLE II
RELATIVE ERROR BETWEEN THE METHOD AND ANSYS

z		1 mm	2 mm	3 mm	4 mm	5 mm
J_r (T)	μ_{ra}	Relative error (%)				
1.10	1.08	3.72	2.94	2.63	2.22	1.00
1.19	1.07	3.33	2.49	2.19	1.79	1.14
1.31	1.14	5.31	4.65	4.35	3.93	2.19
1.40	1.20	6.69	6.07	5.77	5.36	3.62
1.45	1.24	7.78	7.16	6.85	6.46	4.74

Five different permanent magnets are considered. The relative error is calculated to compare the H_z field. Table II shows that the greater the relative permeability, the greater the relative error. Indeed, the unit relative permeability of the magnet is an assumption of the model. The table shows also that the relative errors increase as the study point is closer to the magnet.

IV. SUPERPOSITION PRINCIPLE

To take advantage of the nodal method (9), the magnets must be identical. To apply the linear superposition principle, a reference magnet A_0 is defined (Fig. 3 and Fig. 4). The field produced by a magnet A_1 identical to A_0, but spatially offset, can be calculated using A_0. Indeed, the field produced by A_1 at a target point *C* is the same as the field produced by A_0 at an unknown target point. Two geometrical transformations are proposed to find the position of this target point from the relative position of A_1 with respect to A_0.

A. Translation transformations

Magnet A_1 is identical to the reference magnet A_0 but distant from a vector $\vec{\delta}$ (Fig. 3). The total field at point *C* is the linear superposition of the field of the two magnets at this point:

$$\overrightarrow{H_{tot}^{C}} = \overrightarrow{H_0^C} + \overrightarrow{H_1^C} \tag{10}$$

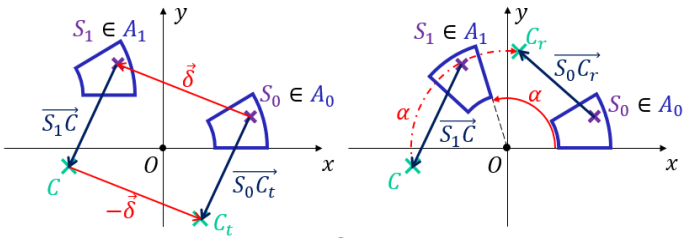

Fig. 3. Translation (left) and rotational (right) transformations

By considering two source points S_0 and S_1 belonging respectively to A_0 and A_1. A new target point C_t is defined as distant by the length δ from point C:

$$\overrightarrow{OC_t} = \overrightarrow{OC} - \delta \quad and \quad \overrightarrow{S_1C} = \overrightarrow{S_0C_t} \tag{11}$$

The formula (10) can then be written:

$$\overrightarrow{H_{tot}^{C}} = \overrightarrow{H_0^C} + \overrightarrow{H_0^{C_t}} \tag{12}$$

B. Rotational transformations

Magnet A_1 is identical to the reference magnet A_0 but separated by an angle α (Fig. 3). The total field at point C is given by (10). S_0 and S_1 are source points belonging respectively to A_0 and A_1. Since the angle between the two magnets is α, then:

$$\overrightarrow{OS_1} = [R_z(\alpha)]\overrightarrow{OS_0} \tag{13}$$

Where $[R_z(\alpha)]$ is the rotation operator of angle α . A new target point C_r is thus defined:

$$\overrightarrow{OC_r} = [R_z(\alpha)]^{-1}\overrightarrow{OC} \quad and \quad [R_z(\alpha)]^{-1}\overrightarrow{S_1C} = \overrightarrow{S_0C_r} \tag{14}$$

Indeed the vector $\overrightarrow{S_1C}$ and $\overrightarrow{S_0C_r}$ have the same norm. The total field is given by:

$$\overrightarrow{H_{tot}^{C}} = \overrightarrow{H_0^C} + [R_z(\alpha)]\overrightarrow{H_0^{C_r}} \tag{15}$$

C. Geometric combinations on the prototype

To apply both transformations to the studied motor, the reference magnet is defined at the center of the first rotor (Fig. 4). The translation vector is then defined:

$$\vec{\delta}_l = \begin{pmatrix} R_{C_a} & 0 & z_l \end{pmatrix}^{\mathrm{T}} \tag{16}$$

The angle α between each magnet is the pole pitch (Table I). The position of the magnets relative to the reference magnet can be defined:

$$\overrightarrow{OS_k^l} = [R_z(\alpha)]^{k-1}\left(\overrightarrow{OS_0} + \vec{\delta}_l\right) \tag{17}$$

The set of target points is then defined on the same model as (11) and (14):

$$\overrightarrow{OC_k^l} = [R_z(\alpha)]^{1-k}\overrightarrow{OC} - \vec{\delta}_l \tag{18}$$

The magnets have the same North-South alternation from one rotor to the other.

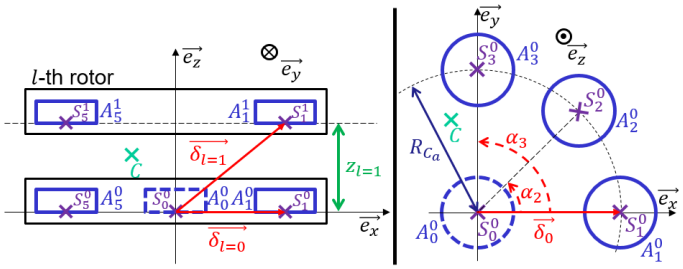

Fig. 4. Position of different magnets relative to the reference magnet A_0^0

It is then possible to write the total magnetic field produced from the field of the reference magnet.

$$\overrightarrow{H_{tot}^{C}} = \sum_{l=0}^{n_r-1}\sum_{k=1}^{2p}(-1)^{k-1}[R_z(\alpha)]^{k-1}\overrightarrow{H_0^{C_k^l}} \tag{19}$$

The total magnetic field (19) is calculated from the field produced by only one magnet (9). The <Q> matrix is calculated only once regardless of the target point C_k^l in (19). For 4050 source points it is possible to calculate all the components of the H field on 192000 target points, distributed in the air gap, in 48.4s with an Intel® Xeon® CPU E3-1271 v3 @ 3.60GHz with 8GB of RAM.

V. Simulations and Experimental Results

A. Test Bench

Static torque is the torque as a function of rotor position for a given DC current supply. It is an electromechanical characteristic of a self-controlled synchronous motor. The static torque generated by the prototype presented in section II is measured on a test bench (Fig. 5). One phase of the motor is supplied with direct current. The rotor is rotated at very low speed. The torque is measured by a force sensor linked to the stator. The experimental static torque C_{exp} is measured at four different supply current values (Table III). When the supplied conductors are between two magnets, the measured torque is null. The torque reaches its extremal values when the supplied conductors are in front of the magnets. In Fig. 7 the initial position of the rotor $-\pi/(2p)$ corresponds to one of the extremal values of the torque. The torque is measured during the forward angular displacement of the rotor from this initial position as shown on Fig. 7.

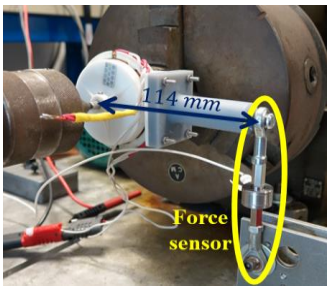

Fig. 5. Torque measurement using a force sensor and a lever arm

B. Finite element analysis

The finite element software ANSYS Electronic desktop is used to calculate the static torque generated by the prototype [11]. All the active parts are represented (Fig. 1). The air box is large enough to consider a null tangential magnetic field on

its external surfaces. The moving band contains the stator. The transient resolution is applied. As for tests, only one phase is supplied. The rotor is moved over a pair of poles. The static torque is calculated for 60 different rotor positions and for four values of the DC current. The total number of mesh elements used is 133574. The CPU time to obtain the static torque C_{3D} by ANSYS presented in Fig. 7 and Table III is 12min57s.

C. Method application

The total magnetic field is calculated by (19) by using the field of the reference magnet shown in Fig 2. The number of source points used is 4050. The number of target points needed to calculate the torque on a pair of poles is 192000. The static torque for each phase is calculated for 60 different rotor positions. Only B_z is shown on Fig. 6 because it allows to calculate the static torque of each phase by the Lorentz force method as explained in [10]. The computation time of the static torque of one phase is 50s.

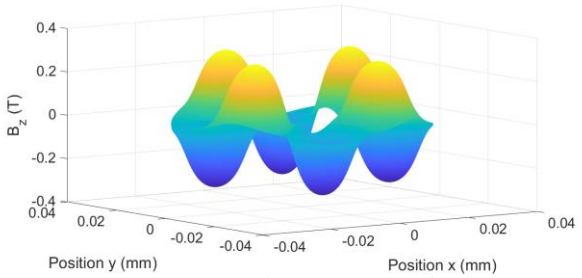

Fig. 6. Total open circuit magnetic field at the center of the coils

The static torque of phase one on a pole pair is shown in Fig. 7. Its maximum values C_{mth} are shown in Table III.

TABLE III
COMPARISON OF STATIC TORQUES FOR ONE PHASE SUPPLIED

I (A)	3	5	7.5	10
Cexp (mN.m)	28.5	48.45	68.4	89.8
C_{3D} (mN.m)	27.25	45.36	68.01	90.66
Cmth (mN.m)	25.2	42.0	62.9	83.9

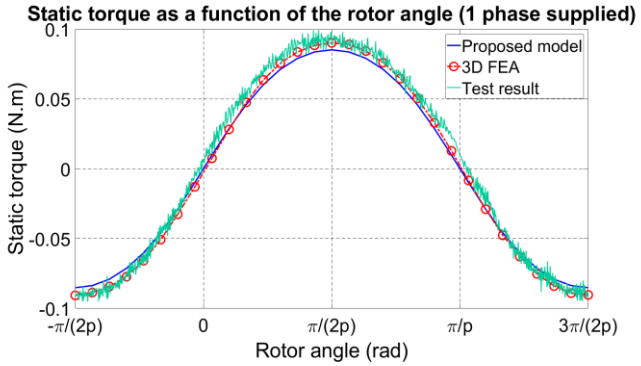

Fig. 7. Comparison for 1 phase supplied with a DC current I = 10A

Differences can be observed between the results of the proposed method and the measurements. From 6.6% to 13.3% relative difference with the prototype. Against 7.46% to 7.52% with ANSYS. This is due to the relative permeability of magnets which is greater than one. Despite these differences, the model remains reliable and the accuracy is acceptable. These magnets with a permeability greater than 1 make it possible to test the limits of the model.

VI. CONCLUSION

The proposed method allows to calculate the open circuit magnetic field of a motor without iron. Its originality is in the writing of the magnetic field of a single magnet in a matrix product which is very fast to perform in Matlab. This writing combined with translation and rotation formulations speed up the field computation.

This method is valid for all magnet and coil geometries, whatever the power supply. If the currents are known in function of the rotor position, the load torque can be calculated in function of the rotor position by linear superposition of the static torque of each phase so the mean torque and the torque ripples can be evaluated. If the rotor speed is known the EMFs can be calculated from the static torque. This method is not able to calculate the AC Joule losses in winding and magnets.

ACKNOWLEDGMENT

Project funded by French Occitanie Région: APR 2018 - Optimotors.

REFERENCES

[1] Z. Zhang, W. Geng, Y. Liu and C. Wang., “Feasibility of a new ironless-stator axial flux permanent magnet machine for aircraft electric propulsion application,” China Electrochemical Society (CES) Transactions on Electrical Machines and Systems., vol. 3, no. 1, 2019.

[2] A. Kampker, P. Treichel, K. Kreisköther, R. Pandey, M. Kleine Büning and T. Backes, “Alternative fabrication strategies for the production of axial flux permanent magnet synchronous motors for enhanced performance characteristics,” IEEE, 8th International Electric Drives Production Conference (EDPC), 2018.

[3] H. Tiismus, A. Kallaste, A. Belahcen, T. Vaimann, A. Rassõlkin, & D. Lukichev (2020). Hysteresis measurements and numerical losses segregation of additively manufactured silicon steel for 3D printing electrical machines. *Applied Sciences*, *10*(18), 6515.

[4] C. Rubeck, J.P. Yonnet, H. Allag, B. Delinchant and O. Chadebec, “Analytical Calculation of Magnet Systems: Magnetic Field Created by Charged Triangles and Polyhedra,” IEEE Transactions on Magnetics, Vol. 49, No. 1, Jan. 2013

[5] R. M. Wojciechowski, “Analysis and optimisation of an axial flux permanent magnet coreless motor based on the field model using the superposition principle and genetic algorithm”, Archives of Electrical Engineering, 2016, vol. 65(3). pp. 601-611.

[6] S. Yazid, H. Menana and B. Douine, "3D Semi-Analytical Modeling and Optimization of Fully HTS Ironless Axial Flux Electrical Machines." *Physica C: Superconductivity and its Applications* (2020): 1353660.

[7] R. Ravaud, G. Lemarquand, and V. Lemarquand. "Ironless permanent magnet motors: Three-dimensional analytical calculation." *2009 IEEE international electric machines and drives conference*. IEEE, 2009.

[8] E. Durand, “Électrostatique Tome I Les distributions”, Masson et Cie, Paris, 1964

[9] G. Dhatt and G. Touzot, “Une presentation de la méthode des éléments finis,” Presses Université Laval, 1981

[10] M. Bonnet, Y. Lefèvre, J.F. Llibre, D. Harribey, F. Defay and N. Sadowski, “3D Magnetic Field Model of a Permanent Magnet Ironless Axial Flux Motor with Additively Manufactured Non-Active Parts,” 19th International Symposium on Electromagnetic Fields in Mechatronics (ISEF), Nancy France, Aug. 2019

[11] ANSYS Corp. ANSYS Electronic Desktop - AED version 18.2, 2017.

[12] Supermagnete, “Physical Magnet Data”, www.supermagnete.fr/eng/physical-magnet-data

[13] Initial Design & Production Prodways, https://www.initial.fr/en/materials/plastics/polyamide-powders.

[14] Dominique Harribey, “3D printed axial brushless motor for drones,” Youtube, https://www.youtube.com/watch?v=JkwLpAAfBVI, 2017